PHOTONICS Research

Review of encapsulation materials for AlGaN-based deep-ultraviolet light-emitting diodes

YOSUKE NAGASAWA AND AKIRA HIRANO*

UV Craftory Co., Ltd., 2-305, Fujimidai 2-7-2, Chikusa-ku, Nagoya 464-0015, Japan
**Corresponding author: hirano@uvcr.jp*

Received 22 January 2019; revised 5 April 2019; accepted 2 May 2019; posted 25 June 2019 (Doc. ID 358390); published 1 August 2019

This paper reviews and introduces the techniques for boosting the light-extraction efficiency (LEE) of AlGaN-based deep-ultraviolet (DUV: $\lambda < 300$ nm) light-emitting diodes (LEDs) on the basis of the discussion of their molecular structures and optical characteristics, focusing on organoencapsulation materials. Comparisons of various fluororesins, silicone resin, and nonorgano materials are described. The only usable organomaterial for encapsulating DUV-LEDs is currently considered to be polymerized perfluoro(4-vinyloxy-1-butene) (p-BVE) terminated with a $-CF_3$ end group. By forming hemispherical lenses on DUV-LED dies using p-BVE having a $-CF_3$ end group with a refractive index of about 1.35, the LEE was improved by 1.5-fold, demonstrating a cost-feasible packaging technique.

https://doi.org/10.1364/PRJ.7.000B55

1. INTRODUCTION

AlGaN-based light-emitting diodes (LEDs) are ultraviolet (UV) light sources tunable between 365 and 200 nm, and early-stage demonstrations of these LEDs were reported in Refs. [1–8]. Due to the advantage of being mercury-free, AlGaN-based LEDs are expected to be an alternative to mercury lamps. To date, deep-ultraviolet (DUV)-LEDs with wavelengths between 255 and 310 nm have been demonstrated by manufacturers [9–13]. Although AlGaN-based DUV-LEDs are expected to be used for sterilization and curing applications, conventional high- and ultrahigh-pressure mercury lamps have a wall-plug efficiency (WPE) of about 10%–15% and low-pressure mercury lamps have a WPE of about 25%. For the bare dies of AlGaN-based DUV-LEDs on sapphire substrates, the reported WPEs have been about 5% [14]. Thus, the development of a technique to improve the WPE is a high priority. The WPE η_{WPE} is expressed as

$$\eta_{\mathrm{WPE}} = (E_p/V_f) \times \eta_{\mathrm{EQE}}, \tag{1}$$

$$\eta_{\mathrm{EQE}} = \eta_{\mathrm{CIE}} \times \eta_{\mathrm{IQE}} \times \eta_{\mathrm{LEE}}. \tag{2}$$

Here, E_p is the luminescence photon energy (eV), and V_f is the forward voltage of the LED. η_{EQE}, η_{CIE}, η_{IQE}, and η_{LEE} denote the external quantum efficiency (EQE), current injection efficiency (CIE), internal quantum efficiency (IQE), and light-extraction efficiency (LEE), respectively. CIE is the ratio of the number of minority carriers injected into the quantum wells (QWs) to the total number of carriers injected into the LED die. IQE is the ratio of the number of generated photons to the number of minority carriers injected into the QWs, which expresses the effect of nonradiative recombination in QWs. LEE is the ratio of the number of photons extracted from LED dies to the number of photons generated in the QWs. The LEE indicates the proportion of usable light because generated light is wasted, mainly due to absorption loss in the devices. EQE is given by multiplying CIE, IQE, and LEE and expresses the ratio of the number of usable photons to the number of carriers injected into the device. It is possible to determine EQEs and WPEs using an integrated sphere and a standard light source. The margins of improvement in IQE, CIE, LEE, EQE, and WPE are overviewed in the following.

IQEs are approximately estimated from the nonsaturated conditions of laser pumping [15,16] or from current–luminescence characteristics [17] of LED devices. In the wavelength region for highly efficient DUV-LEDs between 260 and 300 nm [14,18], estimated IQEs often have exceeded 50% [14,19–21] or been near 50% [16]. Also, the electrical efficiency, which is given by multiplying CIE and IQE, has been estimated to be around 60% [9] in the wavelength region between 280 and 300 nm, meaning that CIEs and IQEs of higher than 60% have been achieved for the bare dies of 285 nm LEDs. The ray-tracing calculation of LEE is currently limited to simulations neglecting the roughness of the diced dies and the nonflat interface of the device layers in the LED. However, an LEE exceeding 10% for bare dies with a p-GaN contact layer on a sapphire substrate has not yet been reported [9]. Indeed, a large margin of improvement in LEE remains compared with those in IQE and CIE.

To improve LEE, various approaches to reduce the absorption loss in p-GaN contact or p-AlGaN cladding layers

have been reported. There are approaches that use reflective p-contacts with a p-reflective contact [22] and encapsulation; EQEs of 20% [23] and 10% [24] are considered to be achievable by increasing LEE. However, all of the reports mentioned an increase in V_f due to the insufficient electrical properties of the p-AlGaN cladding layer and the highly resistive p-contact. Thus, the improvement in WPE was significantly canceled by the increase in V_f. Furthermore, the lifetime of DUV-LEDs tends to decrease in the case of using p-AlGaN cladding and contact layers. Although a decrease in lifetime was measured by making a meshed p-GaN contact layer on p-AlGaN, the decrease in optical output of the DUV-LEDs became larger [22]. At present, a practical approach to improve LEE is to use encapsulation [25] or lens-coupling [26] to utilize the light traveling from the QWs towards the light-extraction surface and the atmosphere. To distinguish the improvement in LEE using a lenslike structure, the improvements in LEE are listed in the tables. Table 1 shows the LEE enhancement ratios obtained without reflective electrodes. Regarding the durability against DUV light, durability of over 5000 h [11] for unknown organomaterials and that of over 6000 h for a fluororesin [27] have been reported. Also, a technique for coupling with a nonorgano quartz or sapphire lens [26] is considered to provide durability against DUV light.

As shown in the tables, the improvement of LEE can be recognized as a priority problem to be solved. In Table 2, the initial performances of the reflective electrode also show a large margin to improve LEE, although it is difficult to expect DUV-LEDs with a practical lifetime in the case of using p-reflective electrodes. On the other hand, when focusing on encapsulation, silicone [(—O—Si—)$_n$] resin did not show sufficient reliability against DUV light [27]. Also, no papers have commented on the lifetime of devices fabricated using silicone. In fact, in a catalog of high-power 365 nm LEDs fabricated by a major manufacturer [28], the window material is limited to hard glass, and this manufacturer limits the use of silicone to LEDs with wavelengths of $\lambda \geq 375$ nm. To our knowledge, the reports on DUV-LEDs employing durable polymers along with their molecular structures are limited to our papers [25,27,29]. One of the aims of this paper is to clarify a suitable molecular structure of the organoencapsulation material by describing the detailed degradation mechanism of resins induced by DUV light on the basis of additional data. Finally, the feasibility of mass-producing packaged devices is demonstrated.

2. SILICONE RESIN

A manufacturer of InGaN-based 365 nm LEDs is mass-producing packaged devices with a quartz window attached on a ceramic container. 365 nm LEDs are being targeted as an alternative to the i-line of high- or ultrahigh-pressure mercury lamps [28]. Several papers have reported devices using silicone resins [23,30]. With this background, we investigated whether silicone resins can be used for encapsulation [27]. As a result, a silicone resin having methyl groups adjacent to Si atoms, for which the silicone structure is considered to be the most robust against UV light, exhibited cracks after a reliability test on a 301 nm LED for 1050 h when the LED was operated at 400 mA. For LEDs with wavelengths of 270 and 287 nm, cracks occurred earlier than for the 301 nm LED at lower operation currents of between 200 and 250 mA and in shorter reliability tests (see details in Ref. [27]). Although the basic structure of silicone is considered to be sufficiently robust against DUV light, cracks are considered to be caused by undesired polymerization due to the activation of the polymerization initiator by the DUV light during the reliability test. Since the polymerization initiator is a catalyst used to synthesize the silicone resin from the siloxane precursors, the

Table 1. LEE Enhancement Ratios Obtained Using Encapsulation or a Lens[a]

Material	Refractive Index	LEE Enhancement Ratio (Shape)	Resin Reliability (Option)	Group	Ref.
Unknown*	1.4	2 (hemisphere)	[5000 h (270 nm)]	Crystal IS	[11]
Silicone*	{1.4}	1.3	n/a	RIKEN	[23]
Silicone	1.4	n/a	<1050 h (D) (301 nm)	UV Craftory	[27]
Fluororesin	1.35	1.5 (hemisphere)	>3000 h (D) (265 nm)	UV Craftory	[25]
Fluororesin	1.35	1.5 (hemisphere)	>6000 h (D) (265 nm)	UV Craftory	[27]
Sapphire lens	1.8	1.9–2.2 (hemisphere)	>1000 h (D) (280 nm)	Nichia	[26]
Unknown	n/a	1.33	n/a (278 nm)	SETi	[31]

[a][ ] = Material test without fabricating devices.
D = Lifetime of the material obtained by fabricating packaged devices.
* = Effect of roughening or reflective electrode is not included.
{ } = Explicit refractive index is not given.

Table 2. LEE Enhancement Ratios with Reflective Electrodes Are Separately Given[a]

Material	Refractive Index	Total LEE Enhancement/ Reliability Test	LEE Enhancement Technique	Group	Ref.
Unknown	n/a	3.3 n/a	p-reflective contact + encapsulation	SETi	[31]
Silicone	{1.4}	4.7 n/a	p-reflective contact + PSS substrate + encapsulation	RIKEN	[23]
Without encapsulation	–	1.55 > 1000 h (at 20 mA)	Meshed p-GaN electrode + n-reflective contact	UV Craftory	[22]

[a]Due to commercial confidentiality, the encapsulation material is not indicated for several cases.
{ } = Not explicitly given in the references. The expected value for the encapsulation material is shown.

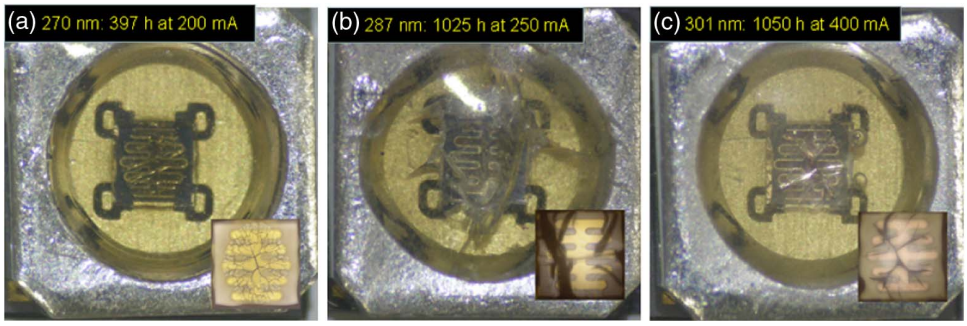

Fig. 1. Cracks in silicone encapsulation of AlGaN-based (a) 270 nm, (b) 287 nm, and (c) 301 nm LEDs after the reliability tests. The time and the operation current during the reliability tests are indicated at the top of the photographs. The insets are magnified images of the cracks. [Figure 1(c) is taken from Ref. [27]. Copyright Japan Society of Applied Physics.]

polymerization initiator should be dispersed uniformly in the bulk. Thus, eliminating the polymerization initiator from the silicone is difficult. Figures 1(a)–1(c) illustrate the cracks in the silicone encapsulation on 270, 287, and 301 nm LED dies after the reliability tests for 397, 1025, and 1050 h, respectively. Figure 2 shows the absorption spectrum for silicone with a carefully chosen polymerization initiator, with the molecular structure of the silicone having side chains of methyl groups shown in the inset. Although this silicone did not show significant absorptance at wavelengths below 250 nm, the occurrence of cracks implies that this silicone is unsuitable for encapsulating DUV-LEDs, even though it was carefully chosen.

3. FLUORINE RESINS

A. Candidate Amorphous Fluororesins Having Transparency in DUV Region

The binding energies of C—H, S—O, and C—F are 408.6–411, 443.7–452, and 482.2–485 kJ/mol [32,33], which correspond

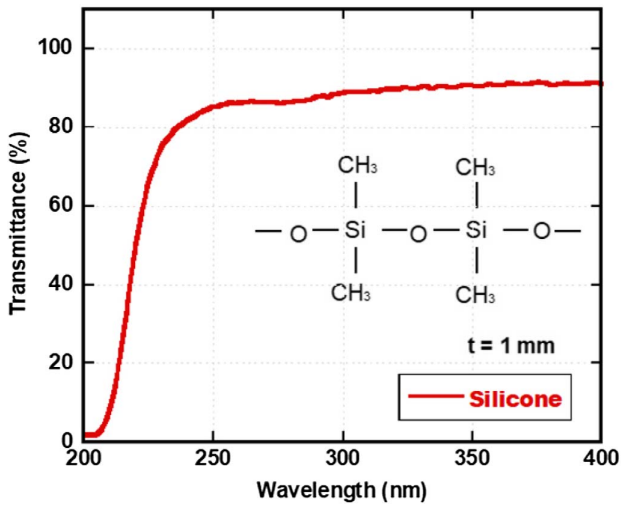

Fig. 2. Absorption spectrum of silicone with side chains of methyl groups with the molecular structure shown as an inset. The weak absorption observed between approximately 250 and 280 nm is considered to be that of the polymerization initiator. (Reproduced from Ref. [27]; copyright Japan Society of Applied Physics.)

to photon energies of 301–303.5, 274–279.5, and 256–257.1 nm, respectively. However, the binding energy depends on the neighboring molecule and the molecular structure. The publicly available binding energies are considered to be criteria for the photoinduced decomposition. The C—F structure is generally stronger than Si—O, and a C—F-based resin can potentially be used as an encapsulation material. A well-known C—F-based polymer is poly(tetrafluoroethylene) (PTFE:[—CF_2—]$_n$), whose structure is similar to that of polyethylene (PE:[—CH_2—]$_n$). PTFE is synthesized from tetrafluoroethylene (TFE:[CF_2=CF_2]). Both PE and PTFE are white in the form of their bulk polymers. The origin of the white color is the scattered light due to the crystallization of the polymer in the case of a straight simple molecular structure, which is a fatal disadvantage for encapsulated LEDs. Another disadvantage of PTFE is the absence of a solvent. To prevent crystallization, a structure protruding from the straight structure is effective. Since fluoropolymers are generally synthesized from TFE, five-membered ring structures can be formed [34,35]. Fluoropolymers with five-membered rings of (—C—C—O—C—O—), having two oxygen atoms [35], and (—C—C—C—O—C), having a single oxygen atom [34], are currently commercially available amorphous fluoropolymers having transparency below 300 nm [36]. The former is synthesized by the copolymerization of TFE and [perfluoro-2,2-dimethyl-1,3-dioxole] (PDD) (PDD-co-TFE). The latter can be synthesized by polymerizing perfluoro(4-vinyloxy-1-butene) (BVE). Since polymerized BVE (p-BVE) is synthesized from TFE using a C—H-based polymerization initiator, the polymerization initiator is decomposed during the polymerization. Thus, undesired polymerization induced by DUV light does not occur, which is an essential difference from the case of silicone. PDD-co-TFE incorporates the (—CF_2—) structure, and the ratio of (—CF_2—) in the main chain is limited to about 35% to prevent crystallization. For p-BVE, the main chain consists of BVE, and all variations of the p-BVE bulk have an amorphous structure. Thus, the protrusion of the five-membered rings makes the bulk fluororesin transparent with absorption edges around 220–250 nm when the terminal end molecules are appropriately chosen. Furthermore, tris(trifluoromethyl) lamine $(CF_3)_3N$ is a typical solvent for both BVE and PDD-co-TFE, which enables them to form flexible shapes.

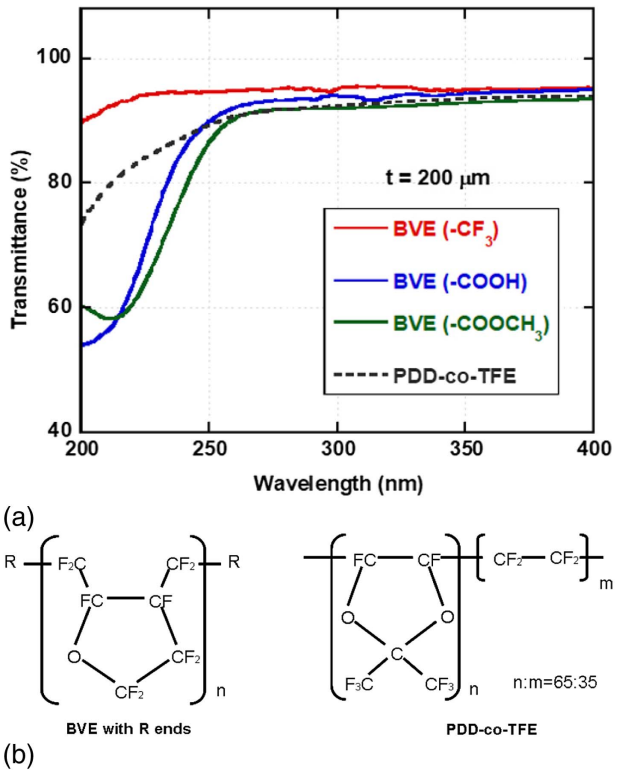

Fig. 3. (a) Transmittance spectra of p-BVEs with various end groups and PDD-co-TEF; (b) molecular structures of (left) p-BVEs with (—R) (R = —COOH, —$COOCH_3$, and —CF_3) end groups and (right) molecular structure of PDD-co-TFE. (Figure 3 is reproduced from Refs. [25,27], copyright Japan Society of Applied Physics; and Ref. [30], copyright Wiley-VCH Verlag GmbH.)

In addition, the modification of the end molecule of the chain structure is possible. A series of p-BVEs with different end groups (—R) of carboxylic acid (—COOH), methyl ester (—$COOCH_3$), and trifluoromethyl (—CF_3) were prepared and compared [27] because these end groups have significant transmittance in the DUV region. Figure 3 shows the transmittance of the p-BVEs with —COOH, —$COOCH_3$, and —CF_3 end groups and PDD-co-TFE terminated with PDD or —CF_3 [35].

B. Comparison of End Groups

To determine the possible molecular structures of suitable amorphous fluororesins, the terminal molecules were investigated using p-BVE with various end groups. Figure 4 shows photographs of the damage to electrodes for various end groups of p-BVE after reliability tests. Except for the case of the —CF_3 end group, damage to the electrode was observed, and serious leakage occurred. In the case of —COOH and —$COOCH_3$ end groups, damage to the electrode occurred after the operation of 265 nm LEDs for 95 and 397 h at 20 mA, respectively. During the reliability tests, the 265 nm LED was operated under a low optical output of a few milliwatts' order. Even in the case of a 285 nm LED using p-BVE with the —COOH end group, damage to the electrode was observed after 804 h (see details in Ref. [25]). In contrast, the p-BVE with the —CF_3 end group did not show any visible electrode damage after 1033 h of operation for a 265 nm LED. The p-BVE with the —$COOCH_3$ end group is considered to be less chemically active than that with the —COOH end group [27]. In general, the decomposition of the COO structure is considered to be induced by DUV light.

Figure 5 shows photographs of DUV-LEDs after 20 mA of operation followed by heating to show outgassing from the bulk resin. The outgassing from the bulk resin was observed as bubbles in the cases of —COOH and —$COOCH_3$ end groups. In contrast, in the case of the —CF_3 end group, no bubbles were seen, providing indirect evidence of the decomposition of —COOH and —$COOCH_3$. The transmittance spectra for p-BVE with —COOH and —$COOCH_3$ end groups are shown in Fig. 3(a). The absorption below around 280 nm for p-BVE with —COOH and —$COOCH_3$ end groups is considered to be related to the bubbles. Meanwhile, p-BVE with the —CF_3 end group did not produce bubbles or damage the electrode. The transmittance spectrum for p-BVE with the —CF_3 end group does not show significant absorption between 240 and 300 nm in the DUV region, suggesting that p-BVE with the —CF_3 end group was not involved in the photolysis induced by 265 nm light.

C. Main-Chain Structure

PDD-co-TFE with terminal molecules of PDD or —CF_3 and p-BVE with —CF_3 end groups were compared to determine the main-chain structure [29]. Dies on a submount were wrapped

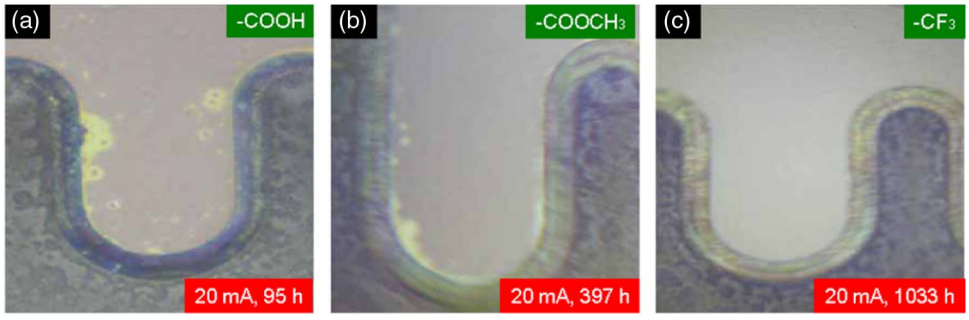

Fig. 4. Photographs of the damage to the electrodes after reliability tests using 265 nm LEDs. A similar phenomenon was observed for p-BVE with the —COOH end group for a 285 nm LED after a reliability test for 804 h [25]. When the damage to the electrodes occurred, a significant increase in the leakage current occurred. (Taken from Ref. [27]; copyright Japan Society of Applied Physics.)

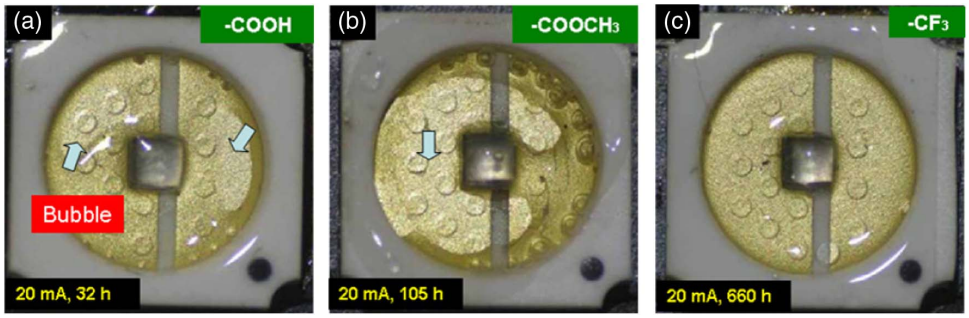

Fig. 5. Bubbles appearing after reliability tests for 32 and 105 h followed by heating up to 230°C for the p-BVE with —COOH and —$COOCH_3$ end groups, respectively. The reliability tests were carried out using 265 nm LEDs under an operation current of 20 mA. [Figures 5(a) and 5(c) are taken from Ref. [27]; copyright Japan Society of Applied Physics. Figure 5(b) is taken from Ref. [37]; copyright is shared by the authors and SPIE.]

using PDD-co-TFE and p-BVE with —CF_3 end groups. These samples were used to compare the main-chain components. In Section 3.B, a comparison of the end groups was performed under 20 mA of operation; however, the investigation of the main-chain structure needed 200 and 350 mA operation for 262 and 289 nm LED dies, respectively, meaning that a much larger dose of DUV light was necessary to damage the electrode and increase the leakage current. For the 262 nm LED, p-BVE did not result in any visible damage to the electrode after the reliability test for 3137 h, as shown in Fig. 6. The increased leakage was confirmed for the case of PDD-co-TFE using the 262 nm LED after 832 h of operation. For the case of the 289 nm LED wrapped with PDD-co-TFE, similar damage to the electrode was observed after the reliability test for 4100 h (see details in Ref. [29]), although the cause of the increased leakage was not definitively determined for the 289 nm LEDs. Thus, PDD with the (C—O—C—O—C) structure is considered to be decomposed by DUV light. The dose of DUV irradiation until the electrode was damaged for PDD-co-TFE was 2 orders larger than those for the —COOH and —$COOCH_3$ end groups. This means that the five-membered PDD ring is stabler than —COOH or —$COOCH_3$. However, PDD, —COOH, and —$COOCH_3$ all have the (—O—C—O—) or (O═C—O—) structure, incorporating two oxygen atoms adjacent to the carbon atom, and are considered to be unsuitable as an encapsulation material for DUV-LEDs, because the local dipole moment of carbon with two neighboring oxygen atoms is considered to play a key role in the photolysis. Accordingly, a possible main-chain component is determined to be p-BVE with a —CF_3 end group.

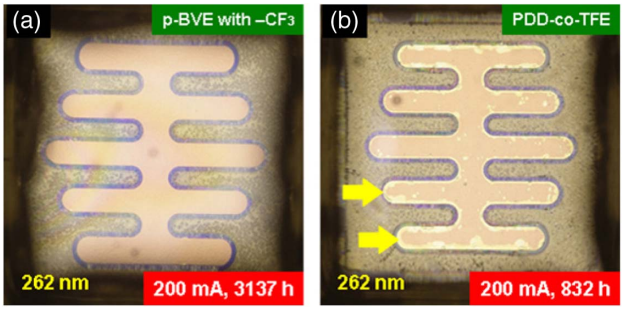

Fig. 6. Damage to the electrodes after reliability tests for 3137 and 832 h at a driving current of 200 mA for 262 nm LEDs wrapped with (a) p-BVE with the —CF_3 end group and (b) PDD-co-TFE. Similar damage to the electrode was observed on a 289 nm LED when using PDD-co-TFE [29]. (Taken from Ref. [29]; copyright Wiley-VCH Verlag GmbH.)

4. DUV-INDUCED PHOTOLYSIS OF FLUORINE RESINS

A. Approaches to Analyzing the Photolysis Induced by DUV Light

To investigate the photolysis of p-BVE with a —COOH end group and PDD-co-TFE induced by DUV light, three types of fluororesins, including p-BVE with a —CF_3 end group as a reference sample, were put in the sample container of a temperature-programmed desorption mass-spectrometry (TPD-MS) system. Using a 261 nm DUV-LED bare die as a light source, samples were prepared with and without the irradiation of the 261 nm LED to determine the species generated by the DUV irradiation treatment. The irradiation time for p-BVE with the —COOH end group was 479 h, and the output of the 261 nm LED was set to 1.5 mW [25], which is referred to as the weak irradiation condition in this paper. To show the robustness of p-BVE with the —CF_3 end group against DUV light, a strong irradiation condition of 6.5 mW was applied using the 261 nm LED, which is the same as that for the PDD-co-TFE sample. The irradiation time was 473 h [29]. The distance between the sample and the 261 nm LED was set to 5 mm. To obtain stronger signals, the quantity of the samples was increased in the case of strong irradiation. Thus, the signals of $m/z =$ 18 and 28 for p-BVE with the —CF_3 end group became about 2 times stronger than those in our previous report under the weak irradiation condition [25].

In addition, 200-μm-thick film samples were prepared for analysis by infrared (IR) spectroscopy. Using a Fourier-transform IR (FT-IR) absorption spectrometer, measurement was performed before and after exposure to a 253.7 nm mercury line. FT-IR measurement also enables the species generated by the DUV irradiation to be determined, corroborating the results obtained by the TPD-MS system. The irradiation time for the film samples of the p-BVE with the —COOH or —CF_3 end group and PDD-co-TFE was 12 h. Differential absorptance was obtained by subtracting the FT-IR spectrum without

DUV irradiation from that with DUV irradiation to determine the increase or decrease in the molecular vibrational level.

B. Photolysis of p-BVE with the —COOH End Group

In the case of p-BVE with the —COOH end group, strong CO, CO_2, H_2O, and CFO signals with a peak of the desorption temperature were detected by TPD-MS. In our previous report [25], the weak CFO signal was not shown but is added in this paper. Figure 7(a) shows the result of TPD-MS for p-BVE with the —COOH end group after the weak DUV irradiation, and Fig. 7(b) shows the result of TPD-MS for p-BVE with the $—CF_3$ end group after the strong DUV irradiation. In the case of p-BVE with the —COOH end group, the intensity of the signals at 1774 and 1811 cm^{-1} in the FT-IR spectra, which are assigned to the —COOH end group, decreased after the DUV irradiation [38]. The result given by FT-IR was in agreement with the results of TPD-MS, as shown in Fig. 7(c). In the case of p-BVE with the $—CF_3$ end group, the TPD-MS spectra of CO, CO_2, and occluding H_2O signals after the 261 nm strong DUV irradiation are similar to those in our previous report [25] showing the overlapping TPD-MS spectra before and after the UV irradiation. Accordingly, p-BVE with the $—CF_3$ end group is robust against DUV light. Thus, the main path generating CO, CO_2, and H_2O in the case of the —COOH end group is considered to be as follows:

$$2COOH \rightarrow CO + CO_2 + H_2O. \quad (3)$$

The signal of $m/z = 47$ in the TPD-MS spectra in Fig. 7(a) also indicates CFO generation, which is in agreement with the increased FT-IR peak at 1890 cm^{-1} in Fig. 7(c), which is assigned to CFO [38,39]. In the case of p-BVE with the $—CF_3$ end group, as seen in the TPD-MS spectrum of CFO in Fig. 7(b), a significant signal was not obtained. Thus, the generation of CFO induced by the photolysis of p-BVE with the —COOH end group can also be used to describe the photolysis of p-BVE with the —COOH end group. The CFO signal in the case of p-BVE with the —COOH end group in Figs. 7(a) and 7(c) is considered to be additional evidence of the removal of the —COOH end group. When the —COOH end group is removed, a dangling bond of the ($—CF_2—$) appears. The CFO is considered to be generated when the dangling bond of the ($—CF_2—$) reacts with an oxygen source. The promising oxygen source to the dangling bond of the ($—CF_2—$) end is H_2O, although there are several possible oxygen-containing molecules. On the basis of this idea, CFO is considered to be generated as follows:

$$(—CF—) + H_2O \rightarrow (—F) + CFO + H_2\uparrow. \quad (4)$$

On the basis of the above analyses, the assumed decomposition mechanism of p-BVE with the —COOH end group is shown in Fig. 8.

C. Photolysis of the PDD Ring Structure

The PDD-co-TFE sample used in our work is considered to be terminated by PDD or $—CF_3$ [35]. Thus, a comparison between p-BVE with the $—CF_3$ end group and PDD-co-TFE enables us to compare the robustness of the BVE and PDD ring structures.

In the case of the TPD-MS analysis of PDD-co-TFE, CO_2 and CFO signals were observed after the strong 261 nm DUV-LED irradiation, as shown in Fig. 9(a). No CO signal was identified. The FT-IR spectra were different before and after the 253.7 nm DUV irradiation for 12 h, as shown in Fig. 9(b). A clear CFO peak was observed at 1890 cm^{-1}.

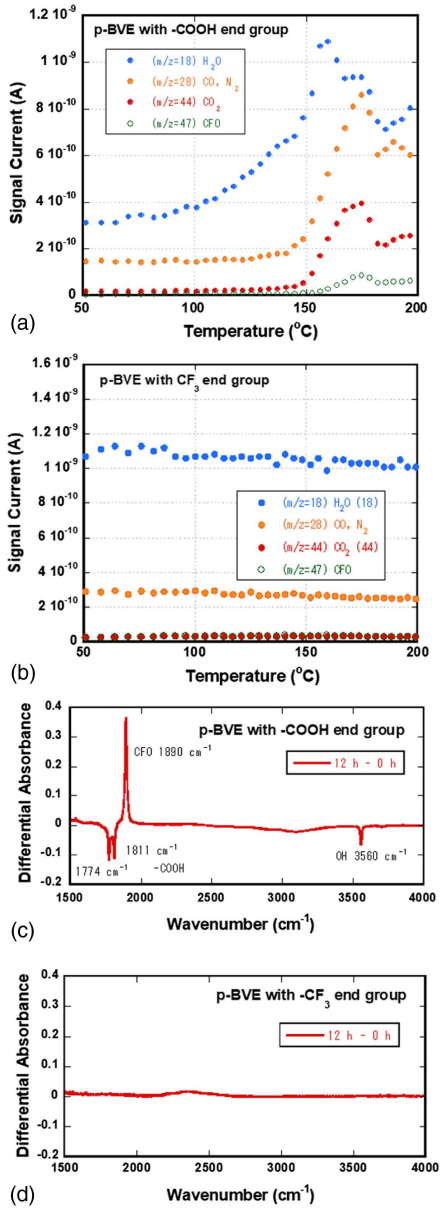

Fig. 7. TPD-MS spectra for H_2O ($m/z = 18$), CO + (N_2) ($m/z = 28$), CO_2 ($m/z = 44$), and CFO ($m/z = 47$) (a) after the weak irradiation treatment using the 261 nm LED for p-BVE with —COOH ends and (b) p-BVE with the $—CF_3$ end group after the strong irradiation treatment, which overlaps those without UV irradiation. Differential FT-IR spectra before and after the 253.7 nm irradiation (c) for p-BVE with the —COOH end group and (d) for p-BVE with the $—CF_3$ end group. The irradiation time was 12 h for p-BVE with the —COOH and $—CF_3$ end groups. Although the CO ($m/z = 28$) signal of TPD-MS cannot be isolated from the background of N_2 ($m/z = 28$), the signal of $m/z = 28$ in (a) has a strong relationship with that of CO_2, which enables us to conclude that the peak curve of $m/z = 28$ is mainly due to the CO signal. [Figure 7(a) is reproduced from Ref. [25] with the CFO signal added.]

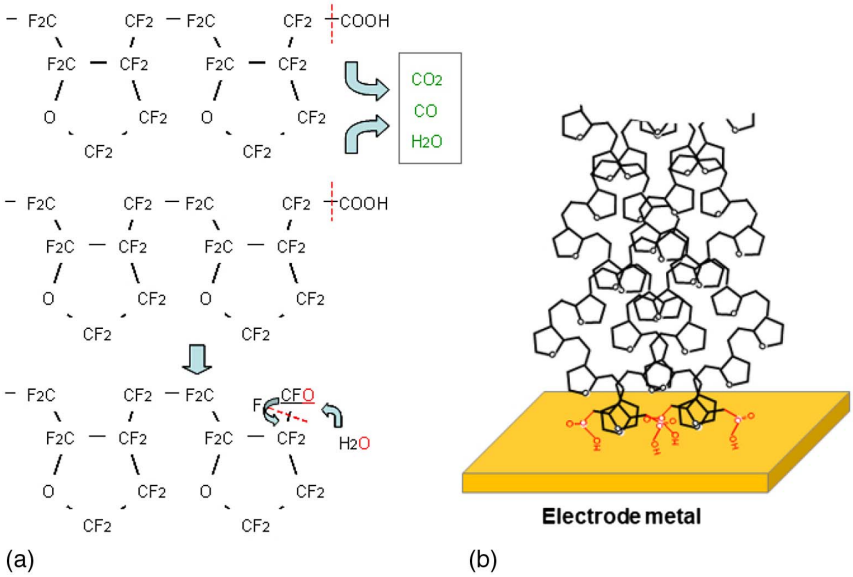

Fig. 8. (a) Decomposition paths for p-BVE with —COOH end group; (b) alignment of the end group on the electrode surface in the case of —COOH. The neighboring —COOH is one of the reasons for the early occurrence of electrode damage in the case of p-BVE with the —COOH end group.

The slight increase at 1860 cm^{-1} is considered to be due to a ketone (>C═O) [40]. Also, an increase in the OH signal intensity was observed at about 3620 cm^{-1}, suggesting that H_2O is related to the decomposition of PDD-co-TFE. From the results of the TPD-MS and FT-IR analyses, the five-membered PDD ring with two oxygen atoms was determined to be decomposed by the DUV irradiation, which was followed by CFO generation [29]. Figure 10(a) shows TPD-MS spectra of $N_2 + CO$ $(m/z = 28)$ and O_2 $(m/z = 32)$ molecules. The TPD-MS signal current of CO_2 in Fig. 9(a) is about 10^{-10} A, and the signal current of $CO + N_2$ $(m/z = 28)$ is about 10^{-9} A. On the basis of the idea that the CO_2 and CO signals are comparable, the signal of $m/z = 28$ can be assigned to be mainly N_2. Also, the TPD-MS spectrum of N $(m/z = 14)$ was similar to that of $m/z = 28$. Thus, the CO signal is considered to be negligible in the $m/z = 28$ signal. In contrast to the result of p-BVE with the $—CF_3$ end group in Fig. 7(b), the signal current of H_2O decreased for PDD-co-TFE after the DUV irradiation, as shown in Fig. 10(b). The decreased amount of H_2O in the bulk PDD-co-TFE suggests that H_2O may be involved in the photolysis of PDD-co-TFE, because the increases in the amount of O_2 and N_2 are considered to be caused by the adsorption from the ambient atmosphere. In addition, the small increase in the OH FT-IR signal intensity, as shown in Fig. 9(b), also led us to consider that H_2O was involved in the decomposition reaction. From the data in Figs. 10(a)–10(b), void creation by the decomposition of the PDD rings in the main chain of PDD-co-TFE can be concluded.

The increases in the TPD-MS signal current of O_2 and N_2 in Fig. 10(a) enable us to explain the void creation in PDD-co-TFE molecules. Note that the O_2 and N_2 TPD-MS spectra do not have a characteristic peak. The TPD-MS spectra without a peak desorption temperature in

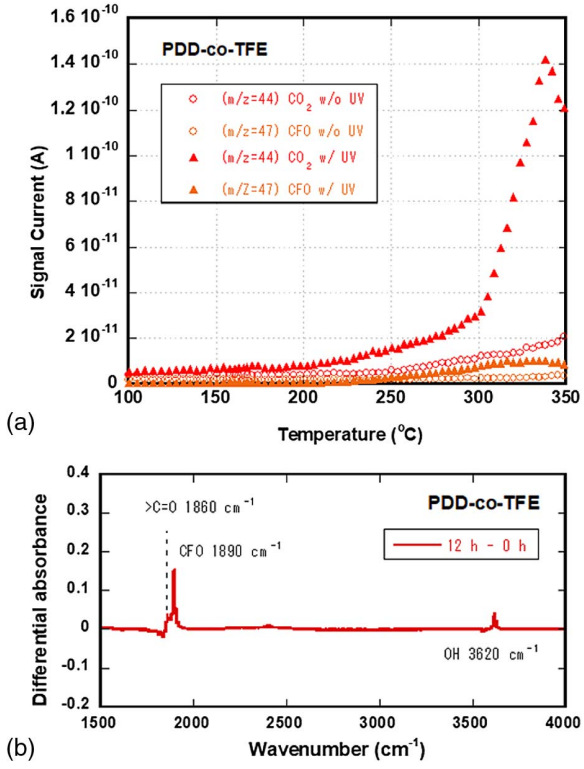

Fig. 9. (a) TPD-MS spectra of CO_2 and CFO for PDD-co-TFE before and after the 261 nm irradiation; (b) differential FT-IR spectrum with a signal of a ketone (>C═O), CFO, and OH after 253.7 nm irradiation for 12 h obtained by subtracting the FT-IR spectrum before the irradiation treatment. The peak at 1890 cm^{-1} can be assigned to CFO and the increase in the signal intensity at 1860 cm^{-1} is assigned to a ketone. The peak at 3620 cm^{-1} is assigned to OH. (Figure 9 is taken from Ref. [29]; copyright Wiley-VCH Verlag GmbH.)

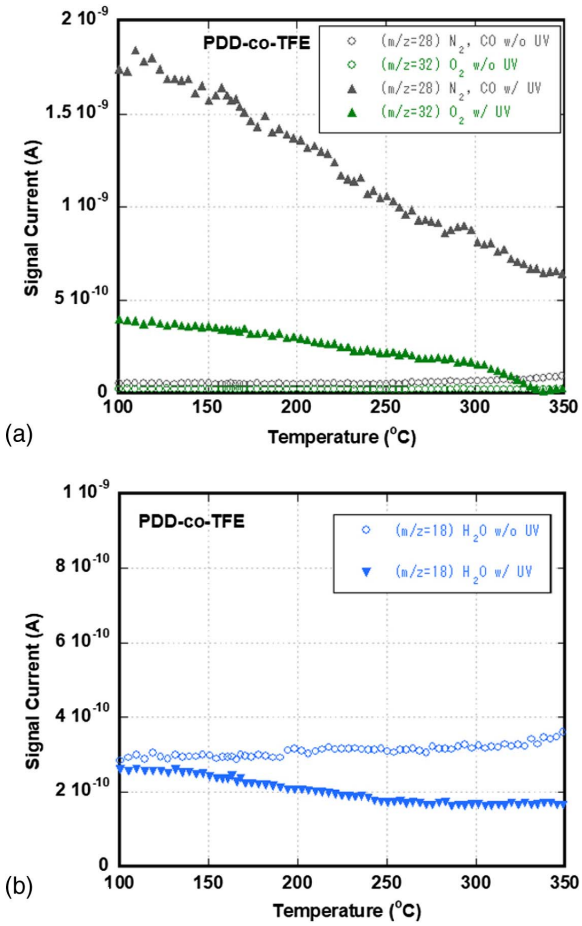

Fig. 10. TPD-MS spectra for (a) N_2 (gray), O_2 (green), and (b) H_2O (blue) before (hollow symbols) and after (solid triangles indicating increases "▲" and decreases "▼") in the irradiation treatment using the 261 nm LED. The markedly increased occlusion of N_2 and O_2 is shown by the increased signal intensity without desorption peaks. The H_2O signal intensity decreased after the irradiation despite the increased occlusion of N_2 and O_2; thus, the source of the oxygen to decompose PDD is likely to be H_2O. The $m/z = 28$ signal current can be attributed mainly to N_2.

Figs. 10(a)–10(b) imply occlusion. Both N_2 and O_2 molecules are sufficiently small compared with the voids corresponding to the five-membered PDD rings. Thus, void creation due to PDD photolysis can be concluded. Figure 11 illustrates the void creation model for PDD-co-TFE with various possible decomposition paths.

On the basis of the TPD-MS and FT-IR spectra in Figs. 9 and 10, the following photolysis model is possible. One possible hypothesis (Case 1: following the arrows from the center of Fig. 11 to the left) is based on the assumption that diperfluoromethylketone [CF_3—CO—CF_3:$(CF_3)_2CO$] is generated, which is based on ketone creation during the photolysis. $(CF_3)_2CO$ is considered to be undetectable because of its low vapor pressure, analogous to the absence of a signal for the solvent $(CF_3)_3N$ in our TPD-MS measurements. After the removal of $(CF_3)_2CO$, one oxygen atom in the ring can create CFO. In this case, the five-membered ring will be entirely broken, and the main chain will be cut, resulting in the creation of voids with a size of the five-membered ring having two —CF_3. In this case, one CFO can be created using the oxygen atom in the ring. The additional CFO can be explained by the external supply of oxygen, such as from H_2O. Another possible decomposition path (Case 2: following the arrows to the right in Fig. 11) is based on the assumption that CO_2 is directly generated from the O—C—O structure in the five-membered ring. In this case, two neighboring free —CF_3 should be created adjacent to the five-membered PDD ring when CO_2 is generated, which should form C_2F_6. C_2F_6 has a high vapor pressure of 3 MPa, possibly resulting in nondetection. In Case 2, an oxygen source is necessary to generate CFO. When oxygen is supplied to the dangling bonds of the polymer after CO_2 removal, the main chain of PDD-co-TFE will be cut, and a void will be created in the bulk resin. In Case 2, there is another possible path for the formation of (—CF═CF—) without cutting the main chain, resulting in the creation of a smaller void. In both cases, it is reasonable to consider the decrease in the TPD-MS spectrum intensity for H_2O after the DUV irradiation. The possible paths for the decomposition are summarized in Fig. 11.

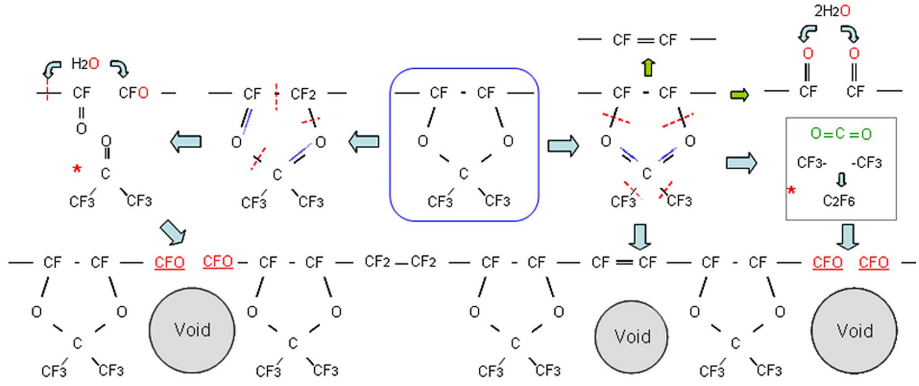

Fig. 11. (Upper) Path for the creation of voids in the case of PDD-co-TFE and (lower) structure after the void creation. The undetectable species due to the high vapor pressure are indicated by "*".

5. EFFECT OF REFRACTIVE INDEX ON INCREASE IN LEE

Figure 12 shows the dependence of the light-extraction enhancement ratio (R_{LEE}) on the refractive index using a hemispherical nonorgano lens or hemisphere resin encapsulation, which includes the results from Refs. [11,25,26] in Table 1(a). Our additional results for the hemispherical quartz lens and silicone encapsulation are additionally given by hollow symbols. All of the data in Fig. 12 are based on devices with a p-GaN contact layer. It is well known that an encapsulation material with a higher refractive index is preferable, as shown in Fig. 12. The refractive index for p-BVE with the $-CF_3$ end group is 1.35 and R_{LEE} is 1.5. In general, an organomolecule with a higher refractive index results in a weaker structure against DUV-induced photolysis. Thus, a different concept is required for further improvement in R_{LEE} using p-BVE. An attempt to increase R_{LEE} by mixing AlN particles has been reported [41]. If the content of the particles is not excessive, p-BVE with the $-COOH$ or $-COOCH_3$ end group can be mixed with ZrO_2 or Al_2O_3 nanoparticles owing to their surface matching with hydrophilic end groups [42]. However, uniform mixing with p-BVE with the $-CF_3$ end group is considered to be difficult because the $-CF_3$ end group only has an affinity to carbon fluoride materials. Generally, it is difficult to obtain a higher refractive index using p-BVE with the $-CF_3$ end group except by the compression of the bulk resin. Accordingly, the improvement of the interface between the sapphire substrate and the p-BVE with the $-CF_3$ end group is considered to be the next priority. For example, the fabrication of nanostructures on sapphire substrates [10] may reduce the loss of light in LED dies. Also, there is a challenge of attaching a sapphire lens on the DVU-LED dies using a technique based on inorganic bonding [26], because an organoadhesive between a nonorgano lens and sapphire is lacking.

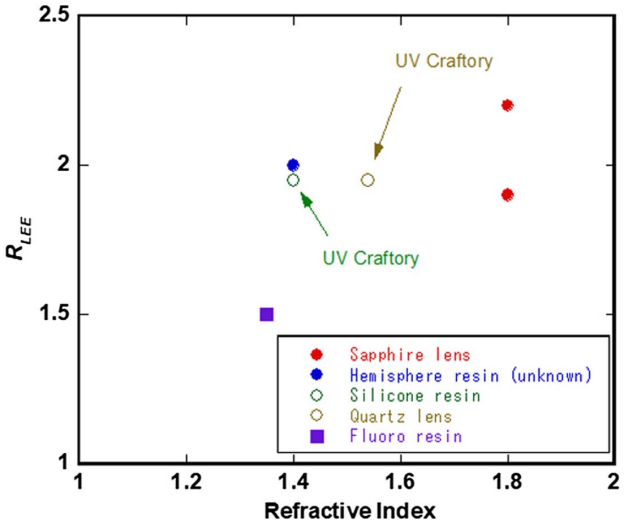

Fig. 12. Light extraction enhancement ratio (R_{LEE}) plotted against the refractive index for different materials. Red solid circles indicate the cases with a hemisphere sapphire lens [26]. The blue solid circle indicates the case of encapsulation with an unknown resin [11]. The violet solid square indicates the case of fluororesin encapsulation [25,27]. Hollow circles indicate the initial R_{LEE} observed in the experiments by the authors.

6. DEMONSTRATION OF MASS PRODUCTION OF ENCAPSULATED LEDS

High- and ultrahigh-pressure mercury lamps cost between 100 and 1000 USD, and provide about 15 W UV light emission. Also, low-pressure mercury lamps providing 4-25 W UV emission cost 30–100 USD. Assuming a power of 100 mW per DUV packaged device, a price of 1–10 USD is considered to make such devices competitive with conventional mercury lamps and will enable DUV-LEDs to be feasible alternatives to mercury lamps. Currently, commercially available DUV-LEDs are mostly based on fully hermetic ceramic packaging [43–45]. However, because a quartz window is attached onto a sintered AlN ceramic container with sidewalls, a significant proportion of the DUV light from the dies is not extracted from the packaging. This packaging loss has been estimated to be 40% [43], and the EQE of packaged commercial DUV-LEDs is currently limited to around 3%, although the bare dies exhibited EQEs of more than 6% between 280 and 300 nm [9]. Also, attaching a reflector onto the submount can reduce the packaging loss [46]. Although a low refractive index such as 1.35 is a fundamental property of fluororesins having robustness to DUV, resin encapsulation will enhance the LEE 1.5-fold [25,27] in addition to reducing the packaging loss. Thus, although R_{LEE} is limited to around 1.5, establishing a mass production technique for devices with fluororesin encapsulation is considered to be a priority, because the device output is expected to be twice that of the conventional packaged devices [14]. Thus, a demonstration of the mass production of 3535 chip-on-submount (COS) packages isolated from a 50.8 mm × 102.4 mm AlN sheet was performed [47]; the results are shown in Fig. 13. A low-viscosity fluoropolymer requires strict control of the surface when a metal mold with hemispherical concaves is used, which may result in DUV-LEDs being uncompetitive with conventional mercury lamps in terms of cost. Thus, the mold of the lens array used in this demonstration was a soft material made of silicone, which can also act as a release agent. The authors believe that this method will contribute to the fabrication of cost-feasible devices.

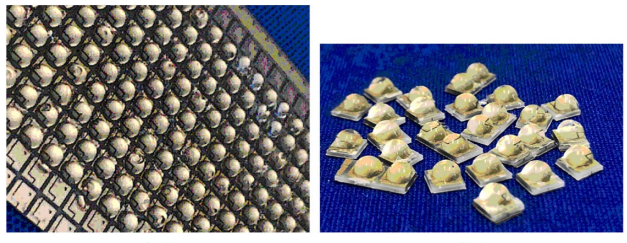

Fig. 13. (a) Photograph of the fabricated lens array on a 50.8 mm × 102.4 mm AlN sheet. (b) Isolated 3535 COS packages. This simple device mount reduces the loss of light resulting from the use of a conventional container-type ceramic package with a quartz window and enhances the light extraction 1.5-fold relative to that of the bare die.

7. SUMMARY

The terminal molecular structure of fluoropolymers that can be used to encapsulate DUV-LEDs is considered to be limited to the $-CF_3$ end group. The absorption with wavelengths of around 280 nm or less arising from (—O—C—O—) or (—O—C═O) structures with two oxygen atoms adjacent to the carbon atom should cause the photolysis of the fluororesin induced by DUV light. Within the current C—F chemistry, the destination of the fluoropolymer synthesized from TFE is limited to five-membered rings incorporating noncarbon atoms in the five-membered ring structure, and a single oxygen atom can be incorporated. Accordingly, p-BVE with the $-CF_3$ end group is currently the only resin that can be used as an encapsulation material for DUV-LEDs.

The disadvantage of this fluoropolymer is its low refractive index of around 1.35. The affinity of p-BVE with the $-CF_3$ end group does not match with a ceramic heat sink or sapphire substrate. Thus, the anchor effect should be utilized. Despite the low refractive index and the difficulty in handling the fluororesin with the $-CF_3$ end group, mass production of a COS package has been demonstrated using a silicone mold and p-BVE with the $-CF_3$ end group. The encapsulated DUV-LEDs are expected to reduce the loss of light due to the wall of a container-type packaging and increase the LEE 1.5-fold. The low refractive index is considered to be a drawback of the fluoropolymer having a DUV transmittance. To further improve the LEE, the authors believe that searching for a way to reduce the loss at the interface between the sapphire and resin is the next priority. For DUV-LEDs to be an alternative to mercury lamps, a semiconductor process such as nanoimprinting, which is suitable for mass production, should be applied to reduce the loss at this interface.

REFERENCES

1. S. Kamiyama, M. Iwaya, S. Takanami, S. Terao, A. Miyazaki, H. Amano, and I. Akasaki, "UV light-emitting diode fabricated on hetero-ELO-grown $Al_{0.22}Ga_{0.78}N$ with low dislocation density," Phys. Status Solidi A **192**, 296–300 (2002).
2. V. Adivarahan, S. Wu, A. Chitnis, R. Pachipulusu, V. Mandavilli, M. Shatalov, J. P. Zhang, M. Asif Khan, G. Tamulaitis, A. Sereika, I. Yilmaz, M. S. Shur, and R. Gaska, "AlGaN single-quantum-well light-emitting diodes with emission at 285 nm," Appl. Phys. Lett. **81**, 3666–3668 (2002).
3. A. Chitnis, J. P. Zhang, V. Adivarahan, W. Shuai, J. Sun, M. Shatalov, J. W. Yang, G. Simin, and M. A. Khan, "324 nm light emitting diodes with milliwatt powers," Jpn. J. Appl. Phys. **41**, L450–L451 (2002).
4. H. Hirayama, Y. Enomoto, A. Kinoshita, A. Hirata, and Y. Aoyagi, "Efficient 230-280 nm emission from high-Al-content AlGaN-based multiquantum wells," Appl. Phys. Lett. **80**, 37–39 (2002).
5. M. Iwaya, S. Takanami, A. Miyazaki, Y. Watanabe, S. Kamiyama, H. Amano, and I. Akasaki, "High-power UV-light-emitting diode on sapphire," Jpn. J. Appl. Phys. **42**, 400–403 (2003).
6. H. Hirayama, T. Yatabe, N. Noguchi, T. Ohashi, and N. Kamata, "231-261 nm AlGaN deep-ultraviolet light-emitting diodes fabricated on AlN multilayer buffers grown by ammonia pulse-flow method on sapphire," Appl. Phys. Lett. **91**, 071901 (2007).
7. Y. Taniyasu, M. Kasu, and T. Makimoto, "An aluminium nitride light-emitting diode with a wavelength of 210 nanometres," Nature **441**, 325–328 (2006).
8. K. Nagamatsu, N. Okada, H. Sugimura, H. Tsuzuki, F. Mori, K. Iida, A. Bando, M. Iwaya, S. Kamiyama, H. Amano, and I. Akasakia, "High-efficiency AlGaN-based UV light-emitting diode on laterally overgrown AlN," J. Cryst. Growth **310**, 2326–2329 (2008).
9. M. Kaneda, C. Pernot, Y. Nagasawa, A. Hirano, M. Ippommatsu, Y. Honda, H. Amano, and I. Akasaki, "Uneven AlGaN multiple quantum well for deep-ultraviolet LEDs grown on macrosteps and impact on electroluminescence spectral output," Jpn. J. Appl. Phys. **56**, 061002 (2017).
10. C. Pernot, M. Kim, S. Fukahori, T. Inazu, T. Fujita, Y. Nagasawa, A. Hirano, M. Ippommatsu, M. Iwaya, S. Kamiyama, I. Akasaki, and H. Amano, "Improved efficiency of 255-280 nm AlGaN-based light-emitting diodes," Appl. Phys. Express **3**, 061004 (2010).
11. J. R. Grandusky, J. F. Chen, S. R. Gibb, M. C. Mendrick, C. G. Moe, L. Rodak, G. A. Garrett, M. Wraback, and M. L. J. Schowalter, "270 nm pseudomorphic ultraviolet light-emitting diodes with over 60 mW continuous wave output power," Appl. Phys. Express **6**, 032101 (2013).
12. A. Fujioka, K. Asada, H. Yamada, T. Ohtsuka, T. Ogawa, T. Kosugi, D. Kishikawa, and T. Mukai, "High-output-power 255/280/310 nm deep ultraviolet light-emitting diodes and their lifetime characteristics," Semicond. Sci. Technol. **29**, 084005 (2014).
13. S. Inoue, T. Naoki, T. Kinoshita, T. Obata, and H. Yanagi, "Light extraction enhancement of 265 nm deep-ultraviolet light-emitting diodes with over 90 mW output power via an AlN hybrid nanostructure," Appl. Phys. Lett. **106**, 131104 (2015).
14. Y. Nagasawa and A. Hirano, "A review of AlGaN-based deep-ultraviolet light-emitting diodes on sapphire," Appl. Sci. **8**, 1264 (2018).
15. K. Ban, J. Yamamoto, K. Takeda, K. Ide, M. Iwaya, T. Takeuchi, S. Kamiyama, I. Akasaki, and H. Amano, "Internal quantum efficiency of whole-composition-range AlGaN multiquantum wells," Appl. Phys. Express **4**, 052101 (2011).
16. H. Murotani, D. Akase, K. Anai, Y. Yamada, H. Miyake, and K. Hiramatsu, "Dependence of internal quantum efficiency on doping region and Si concentration in Al-rich AlGaN quantum wells," Appl. Phys. Lett. **101**, 042110 (2012).
17. H. Yoshida, M. Kuwabara, Y. Yamashita, K. Uchiyama, and H. Kan, "Radiative and nonradiative recombination in an ultraviolet GaN/AlGaN multiple-quantum-well laser diode," Appl. Phys. Lett. **96**, 211122 (2010).
18. M. Kneissl and J. Rass, *III-Nitride UV Emitter: Technologies and Their Applications* (Springer, 2016).
19. C. G. Moe, G. A. Garrett, J. R. Grandusky, J. Chen, L. E. Rodak, P. Rotella, M. Wraback, and L. J. Schowalter, "Correlation between optical and electrical performance of mid-ultraviolet light-emitting diodes on AlN substrates," Phys. Status Solidi **C11**, 786–789 (2014).
20. Z. Bryan, I. Bryan, J. Xie, S. Mita, Z. Sitar, and R. Collazo, "High internal quantum efficiency in AlGaN multiple quantum wells grown on bulk AlN substrates," Appl. Phys. Lett. **106**, 142107 (2015).
21. M. Shatalov, J. Yang, W. Sun, R. Kennedy, R. Gaska, K. Liu, M. Shur, and G. Tamulaitis, "Efficiency of light emission in high aluminum content AlGaN quantum wells," J. Appl. Phys. **105**, 073103 (2009).
22. T. Inazu, S. Fukahori, C. Pernot, M. H. Kim, T. Fujita, Y. Nagasawa, A. Hirano, M. Ippommatsu, M. Iwaya, T. Takeuchi, S. Kamiyama, M. Yamaguchi, Y. Honda, H. Amano, and I. Akasaki, "Improvement of light extraction efficiency for AlGaN-based deep ultraviolet light-emitting diodes," Jpn. J. Appl. Phys. **50**, 122101 (2011).
23. T. Takano, T. Mino, J. Sakai, N. Noguchi, K. Tsubaki, and H. Hirayama, "Deep-ultraviolet light-emitting diodes with external quantum efficiency higher than 20% at 275 nm achieved by improving light-extraction efficiency," Appl. Phys. Express **10**, 031002 (2017).
24. M. Shatalov, W. H. Sun, R. Jain, A. Lunev, X. H. Hu, A. Dobrinsky, Y. Bilenko, J. W. Yang, G. A. Garrett, L. E. Rodak, M. Wraback, M. Shur, and R. Gaska, "High power AlGaN ultraviolet light emitters," Semicond. Sci. Technol. **29**, 084007 (2014).
25. K. Yamada, Y. Furusawan, S. Nagai, A. Hirano, M. Ippommatsu, K. Aosaki, N. Morishima, H. Amano, and I. Akasaki, "Development of underfilling and encapsulation for deep-ultraviolet LEDs," Appl. Phys. Express **8**, 012101 (2015).
26. M. Ichikawa, A. Fujioka, T. Kosugi, S. Endo, H. Sagawa, H. Tamaki, T. Mukai, M. Uomoto, and T. Shimatsu, "High-output-power deep ultraviolet light-emitting diode assembly using direct bonding," Appl. Phys. Express **9**, 072101 (2016).
27. S. Nagai, K. Yamada, A. Hirano, M. Ippommatsu, M. Ito, N. Morishima, K. Aosaki, Y. Honda, H. Amano, and I. Akasaki, "Development of highly durable deep-ultraviolet AlGaN-based LED multichip array with

hemispherical encapsulated structures using a selected resin through a detailed feasibility study," Jpn. J. Appl. Phys. **55**, 082101 (2016)
28. Nichia. 2018, http://www.nichia.co.jp/jp/product/uvled.html.
29. K. Yamada, Y. Nagasawa, S. Nagai, A. Hirano, M. Ippommatsu, K. Aosaki, Y. Honda, H. Amano, and I. Akasaki, "Study on the main-chain structure of amorphous fluorine resins for encapsulating AlGaN-based DUV-LEDs," Phys. Status Solidi **A215**, 1700525 (2018).
30. J. Wu, "High power high efficiency DUV-LEDs and applications," in *LED Taiwan IR+UV Summit* (2016).
31. M. Shatalov, W. Sun, A. Lunev, X. Hu, A. Dobrinsky, Y. Bilenko, J. Yang, M. Shur, R. Gaska, C. Moe, G. Garrett, and M. Wraback, "AlGaN deep-ultraviolet light-emitting diodes with external quantum efficiency above 10%," Appl. Phys. Express **5**, 082101 (2012).
32. http://www.chem.tamu.edu/rgroup/connell/linkfiles/bonds.pdf.
33. http://www.geocities.jp/toyookawase/30ketugoue.pdf.
34. K. Nakamura, N. Sugiyama, Y. Etoh, K. Aosaki, and J. Endo, "Development of perfluoro transparent resins obtained by radical cyclopolymerization for leading-edge electronic and optical applications," Nippon Kagaku Kaishi **12**, 659 (2001).
35. I. Blakey, G. A. George, D. J. T. Hill, H. P. Liu, F. Rasoul, A. K. Whittaker, and P. Zimmerman, "XPS and ^{19}F NMR study of the photodegradation at 157 nm of photolithographic-grade teflon AF thin films," Macromolecules **38**, 4050–4053 (2005).
36. K. Yamamoto and G. Ogawa, "Structure determination of the amorphous perfluorinated homopolymer: poly[perfluoro(4-vinyloxyl-1-butene)]," J. Fluorine Chem. **126**, 1403–1408 (2005).
37. A. Hirano, Y. Nagasawa, M. Ippommatsu, K. Aosaki, Y. Honda, H. Amano, and I. Akasaki, "Development of AlGaN-based deep-ultraviolet (DUV) LEDs focusing on the fluorine resin encapsulation and the prospect of the practical applications," Proc. SPIE **9926**, 99260C (2016).
38. W. K. Fisher and J. C. Correlli, "Effect of ionizing radiation on the chemical composition, crystalline content and structure, and flow properties of polytetorafluoroethylene," J. Polymer Sci. **19**, 2465–2493 (1981).
39. T. R. Dargaville, G. A. George, D. J. T. Hill, U. Scheler, and A. K. Whittaker, "Cross-linking of PFA by electron beam irradiation," Molecules **36**, 7138–7142 (2003).
40. J. Pacansky, R. J. Waltman, and D. Jebens, "Electron beam irradiation of a perfluoroalkoxy fluorocarbon resin: tetorafluoroethylene/perfluoromethyl vinyl ether copolymer," Molecules **29**, 7699–7704 (1996).
41. P. Yang, X. Guo, R. Liang, H. Cheng, and M. Chen, "Enhanced light extraction from DUV-LEDs by AlN-doped fluoropolymer encapsulation," IEEE Photon. Lett. **29**, 1151–1154 (2017).
42. K. Aosaki, personal communication.
43. https://www.nikkiso.co.jp/technology/project/duv-led.html#ac02.
44. https://www.klaran.com/products/uvc-leds/klaran-gd-series.
45. Y. Peng, S. Wang, H. Cheng, and M. Chen, "Whole inorganic hermetic packaging technology using localized induction heating for deep ultraviolet light-emitting diodes," IEEE Trans. Compon. **6**, 1456–1461 (2016).
46. Y. Pai, C. Lin, C. Lee, C. Lin, C. Chen, H. Kuo, and Z. Ye, "Enhancing the light-extraction efficiency of AlGaN-based deep-ultraviolet light-emitting diodes by optimizing the diameter and tilt of the aluminum sidewall," Crystals **8**, 420 (2018).
47. Y. Hatanaka, M. Ito, Y. Sakane, Y. Nagasawa, A. Hirano, and M. Ippommatsu, "Demonstration of mass production techniques at feasible cost for surface mount device of AlGaN-based DUV-LED with fluoro-resin encapsulation," in *International Workshop on Nitride Semiconductors* (2018), paper TuP-OD-2.